J|A|C|S ARTICLES

Published on Web 04/06/2010

Topochemistry and Photomechanical Effects in Crystals of Green Fluorescent Protein-like Chromophores: Effects of Hydrogen Bonding and Crystal Packing

Panče Naumov,*,† Janusz Kowalik,‡ Kyril M. Solntsev,‡ Anthony Baldridge,‡ Jong-Seok Moon,‡ Christine Kranz,§ and Laren M. Tolbert*,‡

Department of Material and Life Science, Graduate School of Engineering, Osaka University, 2-1 Yamada-oka, Suita 565-0871, Osaka, Japan, School of Chemistry and Biochemistry, Georgia Institute of Technology, 901 Atlantic Drive, Atlanta, Georgia 30332-0400, and Institute of Analytical and Bioanalytical Chemistry, University of Ulm, 89081 Ulm, Germany

Received January 31, 2010; E-mail: tolbert@chemistry.gatech.edu; npance@wakate.frc.eng.osaka-u.ac.jp

Abstract: To obtain insight into the effects of the environment on the photophysics and photochemistry of the green fluorescence protein (GFP), eight crystal structures of six synthetic aryl-substituted analogues (2-fluoro, 2-methyl, 3-hydroxy, 3-methoxy, 2,4-dimethyl and 2,5-dimethyl) of the GFP chromophore (4-hydroxy-benzylidenedimethylimidazolinone) were determined and correlated with their two-dimensional steady-state and time-resolved solid-state excitation−emission spectra. The stacking between the molecules greatly affected the emission energy and the lifetime of the emission of the chromophore, implying that $\pi-\pi$ interactions could be critical for the photophysics of GFP. The reaction pathways were dependent on the excitation energy, resulting either in [2 + 2] photodimerization at the bridging double bond (UV excitation) or flipping of the imidazolone ring (visible excitation). The *meta*-hydroxy chromophore (**3-HOBDI**) was the only GFP−chromophore analogue that was obtained as more than one stable polymorph in the pure state thus far. Due to the asymmetric substitution with hydrogen bond donors and acceptors, **3-HOBDI** is tetramorphic, the forms showing distinctly different structure and behavior: (1) while one of the polymorphs (**3-HOBDI**-A), having multilayer structure with alternating stereochemistry of linear hydrogen-bonded motifs, undergoes photodimerization under UV light, (2) another (**3-HOBDI**-C), which has dimeric head-to-tail structure, shows *Z*-to-*E* isomerization via τ-one-bond flip of the imidazolone ring by excitation in the visible region. X-ray diffraction analysis of a partially reacted single crystal of **3-HOBDI**-C provided the first direct evidence of τ-one-bond flip occurring in a GFP-like compound. Moreover, the cooperative action of the photodimerization of **3-HOBDI**-A appears as a photomechanical effect of unprecedented magnitude for a single crystalline specimen, where photoexcited single crystals bend to more than 90° without breaking.

1. Introduction

Fluorescence from the green fluorescent chromophore (GFP) and its derivatives is characterized by a complex ensemble of photophysical phenomena which allow the fluorescence to occur with high quantum yield only within the confines of the protective β-barrel, which inhibits otherwise facile decay pathways. In other environments, including other proteins, fluorescence is in competition with a host of decay pathways, which have been explored by independent synthesis of the chromophores and examination of the photophysics in solution,[1] at low temperature,[2] in the gas-phase,[3] at high pressure,[4] in host−guest complexes,[5] and in the solid state.[6] Of these environments, the environment most analogous to the β-barrel is arguably the solid state. A consistent theme to these studies has been the intervention of twisting modes, both involving the formal double bond and leading to double-bond isomerization and/or the single bond between that bond and the aryl group. Notwithstanding the strong role of the β-barrel in providing a strong restoring force, preventing both facile internal conversion via twisting and double-bond [*trans* (*E*) → *cis* (*Z*)] isomerization, proteins which undergo such isomerization ("photoswitching

† Osaka University.
‡ Georgia Institute of Technology.
§ University of Ulm.

(1) (a) Follenius-Wund, A.; Bourotte, M.; Schmitt, M.; Iyice, F.; Lami, H.; Bourguignon, J.-J.; Haiech, J. *Biophys. J.* **2003**, *85*, 1839–1850. (b) Yang, J.-S.; Huang, G.-J.; Liu, Y.-H.; Peng, S.-M. *Chem. Commun.* **2008**, 1344–1346. (c) Solntsev, K. M.; Poizat, O.; Dong, J.; Rehault, J.; Lou, Y.; Burda, C.; Tolbert, L. M. *J. Phys. Chem. B* **2008**, *112*, 2700–2711. (d) Dong, J.; Abulwerdi, F.; Baldridge, A.; Kowalik, J.; Solntsev, K. M.; Tolbert, L. M. *J. Am. Chem. Soc.* **2008**, *130*, 14096–14098. (e) Vengris, M.; van Stokkum, I. H. M.; He, X.; Bell, A. F.; Tonge, P. J.; van Grondelle, R.; Larsen, D. S. *J. Phys. Chem.* **2004**, *A108*, 4587–4598. For reports on the ultrafast photophysics of the chromophore inside the protein, see (f) Chattoraj, M.; King, B. A.; Bublitz, G. U.; Boxer, S. G. *Proc. Natl. Acad. Sci. U.S.A.* **1996**, *93*, 8362–8367. (g) Lossau, H.; Kummer, A.; Heinecke, R.; Pöllinger-Dammer, F.; Kompa, C.; Bieser, G.; Jonsson, T.; Silva, C. M.; Yang, M. M.; Youvan, D. C.; Michel-Beyerle, M. E. *Chem. Phys.* **1996**, *213*, 1–16. (h) Leiderman, P.; Ben-Ziv, M.; Genosar, L.; Huppert, D.; Solntsev, K. M.; Tolbert, L. M. *J. Phys. Chem. B* **2004**, *108*, 8043–8053. (i) Meech, S. R. *Chem. Soc. Rev.* **2009**, *38*, 2922–2934. (j) van Thor, J. J. *Chem. Soc. Rev.* **2009**, *38*, 2935–2950. (k) Fang, C.; Frontiera, R. R.; Tran, R.; Mathies, R. A. *Nature* **2009**, *462*, 200–204.

(2) (a) Litvinenko, K. L.; Webber, N. M.; Meech, S. R. *J. Phys. Chem. A* **2003**, *107*, 2616–2623. (b) Stavrov, S. S.; Solntsev, K. M.; Tolbert, L. M.; Huppert, D. *J. Am. Chem. Soc.* **2006**, *128*, 1540–1546.

Scheme 1. One-Bond Flip (OBF) and Hula Twist (HT) Mechanisms Suggested for the Photoisomerization of Benzylidenedimethylimidazolinones (BDIs)

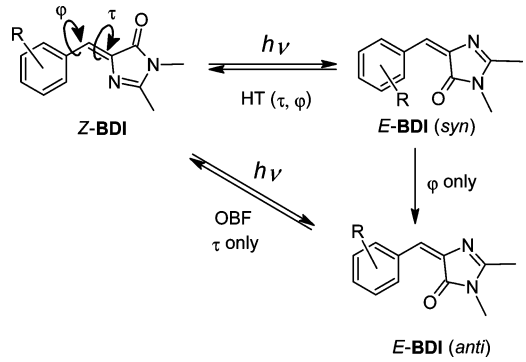

proteins")[7] are now increasingly evident. Concerns about such restraining forces have led to widespread acceptance of the volume-conserving "hula twist",[8] which incorporates simultaneous twisting about dihedral angles τ and φ in the excited-state. This "least-motion" scenario, in order to maintain both aromatic rings in plane, would produce an initial conformer with any *ortho* or *meta* substituents in a *syn* relationship,[9] as opposed to the *anti* relationship in the "one-bond flip" process (see Scheme 1). Thus, we have undertaken a study of such isomerization in the solid state, using derivatives which perturb crystal packing in rationalizable ways. As a result of these investigations, we now report a variety of direct photochemical consequences from the crystal packing, including a remarkable photomechanical effect of the benzylidenedimethylimidazolinone (BDI) chromophores, and additional insight into the possible intervention of the hula twist.

We began these studies with derivatives of the parent chromophore, *p*-hydroxybenzylidenedimethylimidazolinone (**4-HOBDI**).[6] We found that fluorescence "turn-on" occurred in the solid-state for *O*-alkyl derivatives which were almost completely nonfluorescent in solutions. Steady-state and time-resolved emission spectroscopy, as well as X-ray diffraction analysis, revealed the nature of complex emission in the crystals, including the fluorescence of monomers and aggregates. The size of *O*-alkyl substituents played a dramatic role in color tuning of crystalline luminescence. With the increase of alkyl group from methyl to hexyl to dodecyl, the interaction between the aromatic molecules in the lattice became weaker, resulting in a hypsochromic shift in the apparent emission from the crystals. No emission was observed from the unsubstituted hydroxyl derivative, which, unlike the others, was characterized by hydrogen bonding between phenolic OH and the imidazolone carbonyl group. However, none of these molecules exhibited any permanent photochemistry in the solid state, nor could *para* substituents distinguish between the one-bond flip and hula twist processes. In order to further characterize their photophysics, therefore, we undertook a study of molecules for which substituents at the *ortho* and *meta* positions would provide additional stereochemical tags, allowing us to establish whether aryl rotation, at least, was a component of the solid-state chemistry and thus provide direct insight into the hula twist mechanism.

Chart 1. Chemical Structures and Cambridge Structure Database Reference Numbers of the Respective Crystallographic Data of the Six Model GFP Fluorophores[a]

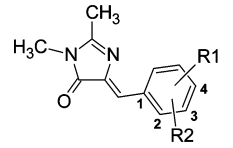

R1	R2	Label	#(CCDC)
3-OH	H	**3-HOBDI**-A[a]	CCDC #761072
3-OCH_3	H	**3-MOBDI**	CCDC #761075
2-F	H	**2-FBDI**	CCDC #761068
2-CH_3	H	**2-MeBDI**	CCDC #761069
2-CH_3	5-CH_3	**2,5-DMBDI**	CCDC #761071
2-CH_3	4-CH_3	**2,4-DMBDI**	CCDC #761070

[a] Polymorphs: CCDC 761073 (form B), CCDC 761074 (form C).

2. Results

2.1. Synthesis, Characterization, and Crystallization. Over 15 BDI chromophores were synthesized according to our previously published protocols.[1d,3b,6] The crystal structures of six representative compounds were determined by single-crystal X-ray diffraction[10] [Chart 1; for crystallographic and refinement details, see Table S1 in the Supporting Information (SI)]. One of these, **3-HOBDI**, produced four polymorphs, three of which were completely structurally characterized and are labeled A,

(3) (a) Andersen, L. H.; Bochenkova, A. V. *Eur. Phys. J.* **2009**, *D51*, 5–14. (b) Rajput, J.; Rahbek, D. B.; Andersen, L. H.; Rocha-Rinza, T.; Christiansen, O.; Bravaya, K. B.; Erokhin, A. V.; Bochenkova, A. V.; Solntsev, K. M.; Dong, J.; Kowalik, J.; Tolbert, L. M.; Åxman Petersen, M.; Brøndsted Nielsen, M. *Phys. Chem. Chem. Phys.* **2009**, *11*, 9996–10002. (c) Forbes, M. W.; Jockusch, R. A. *J. Am. Chem. Soc.* **2009**, *131*, 17038–17039.

(4) Leiderman, P.; Huppert, D.; Remington, S. J.; Tolbert, L. M.; Solntsev, K. M. *Chem. Phys. Lett.* **2008**, *455*, 303–306.

(5) Baldridge, A.; Jayaraj, N.; Samanta, S. R.; Ramamurthy, V.; Tolbert, L. M. *J. Am. Chem. Soc.* **2010**, *132*, 1498–1499.

(6) Dong, J.; Solntsev, K. M.; Tolbert, L. M. *J. Am. Chem. Soc.* **2009**, *131*, 662–670.

(7) (a) Dugave, C., Ed. *Cis-Trans Isomerization in Biochemistry*; Wiley-VCH: Weinheim, 2006. (b) Henderson, J. N.; Ai, H.-W.; Campbell, R. E.; Remington, S. J. *Proc. Natl. Acad. Sci. U.S.A.* **2007**, *104*, 6672–6677. (c) Andresen, M.; Stiel, A. C.; Trowitzsch, S.; Weber, G.; Eggeling, C.; Wahl, M. C.; Hell, S. W.; Jakobs, S. *Proc. Natl. Acad. Sci. U.S.A.* **2007**, *104*, 13005–13009, S13005/13001−S13005/13005. (d) Stiel, A. C.; Trowitzsch, S.; Weber, G.; Andresen, M.; Eggeling, C.; Hell, S. W.; Jakobs, S.; Wahl, M. C. *Biochem. J.* **2007**, *402*, 35–42. (e) Voliani, V.; Bizzarri, R.; Nifos, R.; Abbruzzetti, S.; Grandi, E.; Viappiani, C.; Beltram, F. *J. Phys. Chem.* **2008**, *B112*, 10714–10722. (f) Habuchi, S.; Ando, R.; Dedecker, P.; Verheijen, W.; Mizuno, H.; Miyawaki, A.; Hofkens, J. *Proc. Natl. Acad. U.S.A.* **2005**, *102*, 9511–9516. (g) Usman, A.; Masuhara, H.; Asahi, T. *J. Phys. Chem.* **2006**, *110*, 20085–20088.

(8) (a) Liu, R. S. H.; Yang, L.-Y.; Liu, J. *Photochem. Photobiol.* **2007**, *83*, 2–10. (b) Liu, R. S. H. *Acc. Chem. Res.* **2001**, *34*, 555–562.

(9) Imamoto, Y.; Kuroda, T.; Kataoka, M.; Shevyakov, S.; Krishnamoorthy, G.; Liu, R. S. H. *Angew. Chem., Int. Ed.* **2003**, *42*, 3630–3633.

(10) **2-MeBDI**: $C_{13}H_{14}N_2O$, $M_r = 214.26$, triclinic, $P\bar{1}$, $Z = 2$, $a = 7.2224(2)$ Å, $b = 7.32150(10)$ Å, $c = 12.4936(3)$ Å, $\alpha = 96.8640(10)°$, $\beta = 100.9390(10)°$, $\gamma = 115.8010(10)°$, $V = 568.51(2)$ Å^3; **3-HOBDI**-A: $C_{12}H_{12}N_2O_2$, $M_r = 216.24$, monoclinic, $P2_1/n$, $Z = 8$, $a = 7.555(4)$ Å, $b = 17.172(8)$ Å, $c = 16.754(8)$ Å, $\alpha = 90°$, $\beta = 90.999(12)°$, $\gamma = 90°$, $V = 2173.1(19)$ Å^3; **3-HOBDI**-B: $C_{12}H_{12}N_2O_2$, $M_r = 216.24$, triclinic, $P\bar{1}$, $Z = 4$, $a = 10.2568(3)$ Å, $b = 10.4700(3)$ Å, $c = 12.1996(5)$ Å, $\alpha = 96.512(2)°$, $\beta = 106.279(2)°$, $\gamma = 118.9880(10)°$, $V = 1050.44(6)$ Å^3; **3-HOBDI**-C: $C_{12}H_{12}N_2O_2$, $M_r = 216.24$, triclinic, $P\bar{1}$, $Z = 2$, $a = 7.0404(8)$ Å, $b = 7.2141(7)$ Å, $c = 11.4902(11)$ Å, $\alpha = 74.020(6)°$, $\beta = 80.942(6)°$, $\gamma = 75.193(4)°$, $V = 540.02(10)$ Å^3; **2-FBDI**: $C_{12}H_{11}FN_2O$, $M_r = 218.23$, monoclinic, $P2_1/c$, $Z = 4$, $a = 7.12770(10)$ Å, $b = 11.2873(2)$ Å, $c = 13.6337(2)$ Å, $\alpha = 90°$, $\beta = 105.1860(10)°$, $\gamma = 90°$, $V = 1058.56(3)$ Å^3; **3-MOBDI**: $C_{13}H_{14}N_2O_2$, $M_r = 230.26$, triclinic, $P\bar{1}$, $Z = 2$, $a = 6.9641(3)$ Å, $b = 7.4052(3)$ Å, $c = 12.8203(5)$ Å, $\alpha = 100.458(2)°$, $\beta = 97.239(2)°$, $\gamma = 112.435(2)°$, $V = 586.92(4)$ Å^3; **2,5-DMBDI**: $C_{14}H_{16}N_2O$, $M_r = 228.29$, monoclinic, $P2_1/c$, $Z = 4$, $a = 7.51100(10)$ Å, $b = 21.9578(3)$ Å, $c = 8.04900(10)$ Å, $\alpha = 90°$, $\beta = 110.0470(10)°$, $\gamma = 90°$, $V = 1247.05(3)$ Å^3; **2,4-DMBDI**: $C_{14}H_{16}N_2O$, $M_r = 228.29$, trigonal, $R\bar{3}$, $Z = 18$, $a = 27.911(7)$ Å, $b = 27.911(7)$ Å, $c = 8.407(2)$ Å, $\alpha = 90°$, $\beta = 90°$, $\gamma = 90°$, $V = 5672(3)$ Å^3. The structure of **4-HOBDI**, redetermined in this work, was identical to the one reported previously (ref 6): $C_{12}H_{12}N_2O_2$, $M_r = 216.24$, monoclinic, $P2_1/n$, $Z = 8$, $a = 7.67090(10)$ Å, $b = 16.6594(3)$ Å, $c = 16.9451(3)$ Å, $\alpha = 90°$, $\beta = 91.9170(10)°$, $\gamma = 90°$, $V = 2164.25(6)$ Å^3.

B and C.[11] Form A (**3-HOBDI-**A) has the most distinctive crystal structure, with crystal packing characterized by linear chains of molecules connected by strong hydrogen bonds between the phenolic OH and adjacent imidazolone carbonyls. Photoisomerization of such a supramolecular structure, if done in a single-crystal-to-single-crystal fashion, should favor the intervention of a hula twist in order to maintain the hydrogen-bonding network. We were gratified and surprised to see, not just a photochemical transformation, but also a dramatic photomechanical effect, with rodlike crystals bending upon exposure at angles up to more than 90° without breaking. Of the remaining crystals, four (the other two polymorphs of **3-HOBDI**, **2-FBDI**, and **2,5-DMBDI**, see Chart 1) underwent photoreactions with complete conversion to stable products within minutes, in yields sufficient for NMR characterization. Notably, such photoreactions were accompanied by readily observable photobleaching of the yellow crystals, a phenomenon we had observed occasionally but had not previously investigated.

2.2. Photomechanical Effects in 3-HOBDI-A Crystals. A 0.70 mm × 0.04 mm × 0.01 mm single crystal of **3-HOBDI**-A was mounted at one end on a glass rod with epoxy adhesive (Araldite) and exposed to very weak (<1 mW·cm^{-2}), unfocused, heat-filtered UV light (λ_{max} = 365 nm, with minor contribution from the 313 nm line) from a 250 W medium-pressure Hg lamp (SP-7, Ushio). Upon flashing by UV light (0.1 s), the slender, long crystals of **3-HOBDI**-A underwent a dramatic deformation: the crystals *bent* along their longest axis to >90° without breaking (see Figure 1 and Movie S1 in the SI). As shown in panels b−d of Figure 1, because the crystal curved only during excitation, the angle at the curvature could be controlled by varying the exposure time. At weak excitation power density, the crystal bending ceased in absence of excitation. After more than a minute of continuous or discontinuous irradiation, the crystal had curved more than 90°, before it started to twist due to bending along the second largest axis, until a fracture appeared at the kink and normal to the longest axis (see panels f and g in Figure 1). If flashed or continuously irradiated with stronger UV light (>5 mW·cm^{-2}), nonfixed crystals showed a readily observable photosalient effect: they jumped a few millimeters as a result of acute lattice distortion (see Movie S2 in the SI). This photomechanical effect was observed during a few seconds even after the excitation had been terminated, probably due to latent release of the accumulated structural stress in the crystal lattice. The deformation was plastic, so that the original shape of the crystals was not restored, even after they had been aged in the dark. None of the crystals of the other compounds exhibited similar photomechanical behavior, but thicker crystals of **3-HOBDI**-B, **3-HOBDI**-C, **2-FBDI**, and **2,5-DMBDI**, as well as of the 4-hydroxy derivative, **4-HOBDI** (analogous to the real GFP emitter), tended to crack perpendicular to the longest axis after long-term exposure to UV light.

(11) We have obtained preliminary evidence for the existence of an additional, *fourth* polymorph of **3-HOBDI**, **3-HOBDI**-D. This modification, which has remained poorly characterized, was obtained as very thin, long colorless needle crystals by slow evaporation from ethanol solution at 278 K. The crystals of **3-HOBDI**-D are monoclinic, space group *C*2/*c* (*Z* = 8), with unit cell parameters refined from a limited number of reflections: *a* = 21.5391(99) Å, *b* = 7.0120(32) Å, *c* = 16.4073(75) Å, α = 90°, *β* = 98.860(9)°, *γ* = 90°, *V* = 2448.5 Å^3. The structure contains a single crystallographic type of antiparallel, *anti* molecules of **3-HOBDI** stacked at 3.64 Å. Unlike **3-HOBDI**-B and **3-HOBDI**-C, the molecules do not form dimers; instead, they are monomeric and are connected into pairs by two C−H···O hydrogen bonds between the carbonyl group and one of the methyl groups.

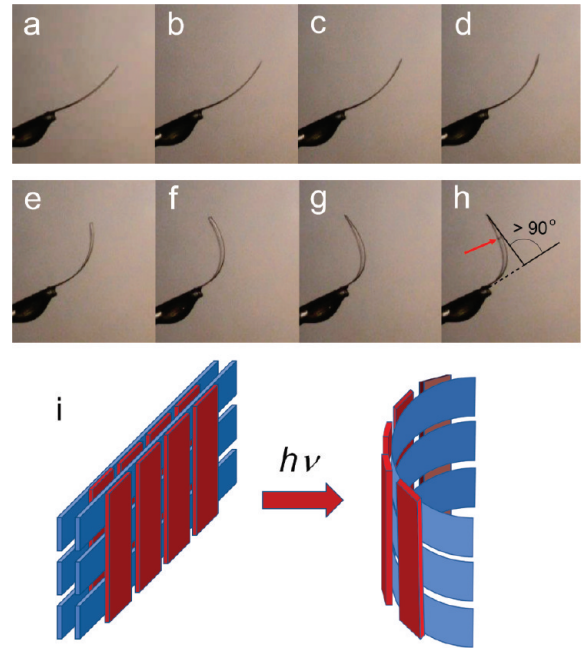

Figure 1. (a−h) Photomechanical effects of the single crystal of **3-HOBDI** exposed to unfocused weak UV light and (i) schematic of the suggested mechanism. The panels b−h show the deformation caused by consecutive exposure (each of b−d corresponds to consecutive 0.1-s flash). Comparison of the panels f and g shows the twisting of the crystal that appears as a result of bending along the smaller axis, after the maximal bending has been reached along the longest axis (the fracture is arrowed in panel h). The perpendicular hydrogen-bonded tapes in the structure are represented schematically in panel i by red and blue ribbons.

UV irradiation (<300 nm, Pyrex-filtered medium pressure 450 W Hg lamp) led to complete quenching of the weak emission of **3-HOBDI**-A at λ^{em} = 440 nm. Upon several 30-s exposures to weak polychromatic UV light (250 W Hg lamp), the IR spectra of powders of **3-HOBDI** (all three structurally characterized polymorphs), **2-FBDI**, **2,5-DMBDI**, and **4-HOBDI** dispersed in KBr showed drastic changes due to gradual and complete conversion to photostable products (Figures S1−S6 in the SI), while the other three compounds remained nonreactive. Most characteristic were the blue-shifts of the ν(CO) and ν(OH) modes (in the case of **3-HOBDI** and **4-HOBDI**): typically, for **3-HOBDI**-A the respective values were $\Delta\tilde{\nu}$ = 17 and 125 cm^{-1}. The reaction of **2-FBDI**, and **2,5-DMBDI** was more rapid relative to **3-HOBDI** and was completed within a minute. The photoreactivity was confirmed by ^{1}H NMR spectra recorded in solid state and in solution (Figure S7 in the SI), and could be also visually observed as bleaching of excited powdered samples.

The reaction product from **3-HOBDI** was purified by removing the soluble starting material with multiple acetone washes. The NMR spectra clearly showed differences between the starting material and the product (Figure S7 in the SI). Most pronounced was the loss of the vinyl double bond, along with appearance of a new two-proton singlet at 3.9 ppm. The signals due to the imidazolone ring were present and slightly shifted from their positions in the starting material. There was no change in the total number of protons in the product compared to those in the starting material. The ^{13}C NMR spectrum indicated a total disappearance of the vinyl carbon atoms and showed the presence of the imidazolone carbon atoms in addition to the appearance of two new signals at approximately 53 and 73 ppm. The total

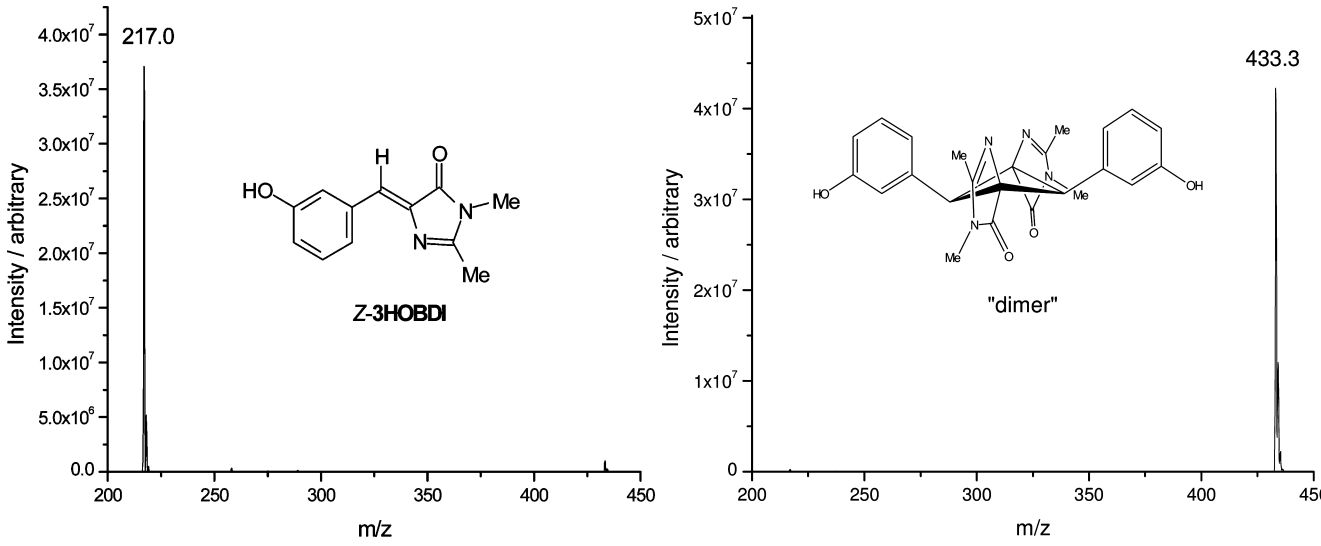

Figure 2. ESI mass spectra of *Z*-**3-HOBDI** and of the dimer.

Scheme 2. Products of Irradiating **3-HOBDI** in Solution and in the Solid State

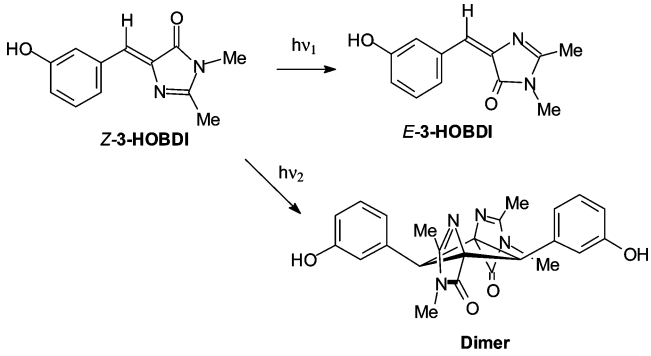

number of distinct carbon atoms remained the same as in the starting material. The ESI spectra of the **3-HOBDI** and the pure dimer show molecular ion signals at 217 $[M+1]^+$ and 433 $[M+1]^+$, respectively (Figure 2). Symmetrical [2 + 2] photodimers of unsaturated compounds have been well characterized as containing either mirror symmetry (C_s) or two-fold symmetry ($C2$).[12] On the basis of the NMR spectrum, we believe that the homodimer of **3-HOBDI** is the two-fold symmetric *trans*,*trans* species (see Scheme 2), although we must concede that we cannot exclude other symmetric dimers. The remaining photoactive derivatives yielded analogous products, in all cases again yielding, presumably, the $C2$-symmetric photodimer.[13]

2.3. Crystal Structures of the BDIs. Polymorph/solvate screening of the six BDIs in Chart 1 afforded four polymorphs of the *m*-hydroxy compound (**3-HOBDI**-A, -B, -C and -D; three of which were characterized),[11] and a single form of each of the other compounds. None of the eight crystal structures characterized by X-ray diffraction analysis[10] included solvent, as expected from the flatness of the BDI molecules and their close packing provided by the molecular stacking (Figure 3). The molecular shape varied from flat (the angle between the two rings is 1.52(11)° in **2,4-DMBDI** and 1.74(2)° in **2-FBDI**) to slightly bent (in the case of **3-HOBDI**-B, 8.49(27) and 8.90(24)°, and **2,5-DMBDI**, 7.86(10)°), so that some of the molecules appeared bow-shaped. The substituents at the phenyl ring did not appear to have significant effect on the intramolecular distances, so that the bridging double bond (1.340(7)−1.350(8) Å) and single bond (1.450(2)−1.462(7) Å) remained essentially constant over all electron-donor and -acceptor substituents. Although the free rotation of the phenyl ring around its axis indicates that both *syn* and *anti* isomers can exist for each of the nonsymmetrically substituted compounds, in all cases where the phenyl ring is substituted with a group which is devoid of an acidic proton (**2-MeBDI**, **2-FBDI**, **3-MOBDI**, **2,5-DMBDI**, **2,4-DMBDI**), the proximate (*ortho* or *meta*) phenyl substituent in the crystals is juxtaposed *anti* in respect to the *ortho*-nitrogen of the imidazole ring. The preferred *anti* orientation is determined by the fact that it leaves the substituents to point outward, turning them accessible for other intermolecular interactions.

To our knowledge, **3-HOBDI** is the only BDI-type molecule that has been crystallized as more than one polymorph (Figure S8 in the SI). At ambient conditions, the majority of sample crystallized as form **3-HOBDI**-A, presumably the thermodynamically most stable structure. Occasionally, a small amount of **3-HOBDI**-B was obtained concomitantly with **3-HOBDI**-A. In a few trials, pure batches of the third form, **3-HOBDI**-C, were obtained. At a molecular level, most apparent factors for the existence of stable polymorphs of **3-HOBDI** at room temperature and their absence in the case of other compounds, despite similar molecular shapes, are the combination of a very asymmetric structure of its nearly planar molecule with hydrogen bond donors (OH) and acceptors (CO and N) in both rings, and the rotational freedom around the C−Ph bond. The overall structure resembles that of the decamorphic compound ROY.[14]

(12) (a) Chung, J. W.; You, Y.; Huh, H. S.; An, B.-K.; Yoon, S.-J.; Kim, S. H.; Lee, S. W.; Park, S. Y. *J. Am. Chem. Soc.* **2009**, *131*, 8163–8172. (b) Yang, S.-Y.; Naumov, P.; Fukuzumi, S. *J. Am. Chem. Soc.* **2009**, *131*, 7247–7249. (c) MacGillivray, L. R.; Papaefstathiou, G. S.; Friščić, T.; Hamilton, T. D.; Bučar, D.-K.; Chu, Q.; Varshney, D. B.; Georgiev, I. G. *Acc. Chem. Res.* **2008**, *41*, 280–291. (d) Georgiev, I. G.; MacGillivray, L. R. *Chem. Soc. Rev.* **2007**, *36*, 1239–1248. (e) Ajamian, A.; Gleason, J. L. *Angew. Chem., Int. Ed.* **2004**, *43*, 3754–3560. (f) Cozzi, P. G. *Chem. Soc. Rev.* **2004**, *33*, 410–421. (g) Cao, G.; Mallouk, T. E. *J. Solid State Chem.* **1991**, *94*, 59–71. (h) Sharma, C. V. K.; Panneerselvam, K.; Shimoni, L.; Katz, H.; Carrell, H. L.; Desiraju, G. R. *Chem. Mater.* **1994**, *6*, 1282–1292.

(13) In retrospect, we now recognize that several of these derivatives showed the presence of "impurities" in purified samples, a phenomenon we can now attribute to the photodimerization and which serves as a caution when handling such compounds in the solid state.

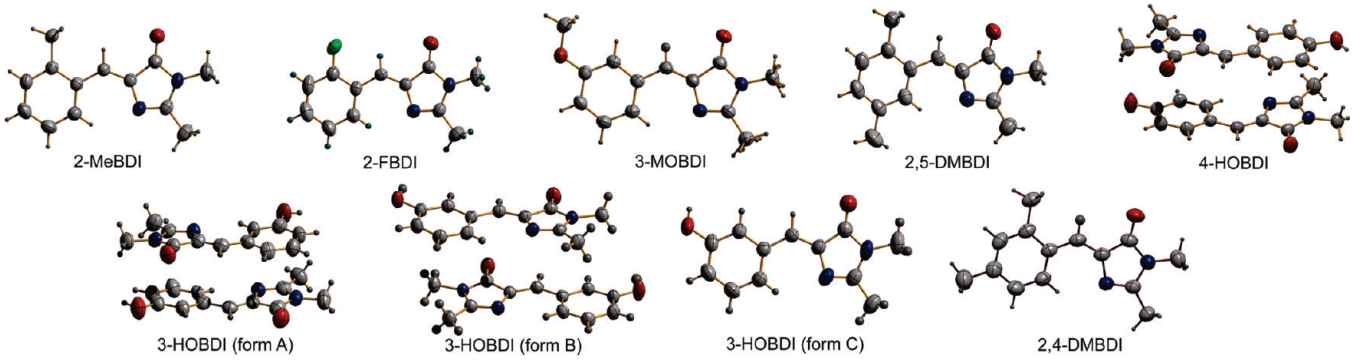

Figure 3. ORTEP-style diagrams, plotted at 50% probability level, of the molecular structures of the substituted BDIs in Chart 1, shown together with that of the GFP emitter, the *para*-hydroxy analogue (**4-HOBDI**, the structure of which was confirmed by redetermination in this work). Both modeled components of the disordered methyl groups in the structure of **3-MOBDI** are shown.

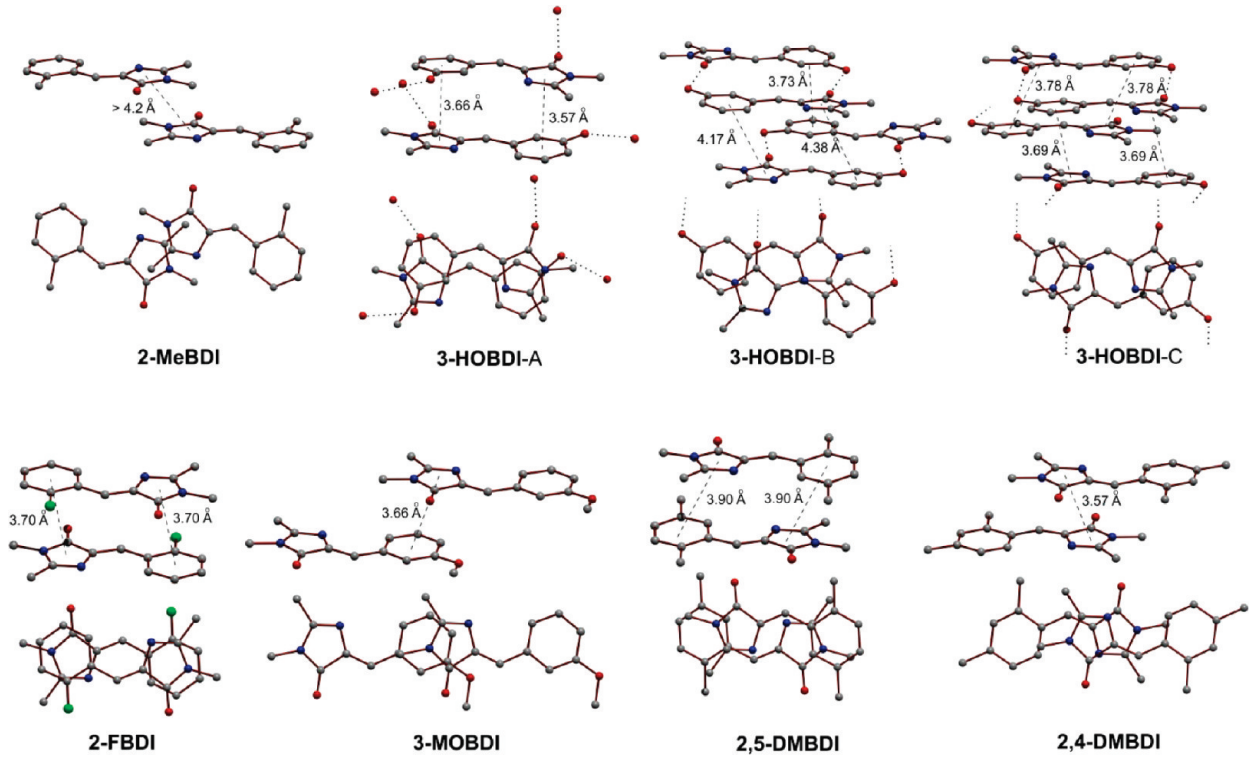

Figure 4. Packing in the crystals of the BDIs showing the relevant center-to-center distances (in angstroms, rounded to ±0.01 Å for clarity) and the relative molecular orientation. From the hydrogen bonds, only the strong O−H···O bonds in the three forms of the 3-hydroxyl derivative (**3-HOBDI**) are shown.

3-HOBDI-A is also the only crystal which contains one of the two structurally different molecules having its phenyl substituent (the hydroxyl group) *syn*-orientated with respect to the imidazolone ring. In contrast to form A, in **3-HOBDI**-B both crystallographic types of molecules are in the *anti* conformation, whereas in **3-HOBDI**-C there is only one *anti* molecule (Figure 3). In the three polymorphs, these two conformations exist as three different hydrogen-bonding patterns: infinite polymeric head-to-tail hydrogen-bonded chains of either *anti* or *syn* molecules similar to **4-HOBDI** in **3-HOBDI**-A,[6] and head-to-tail hydrogen-bonded dimers in **3-HOBDI**-B and **3-HOBDI**-C (see, however, ref 11). The all-*syn* and all-*anti* chains in the crystal of **3-HOBDI**-A are arranged into alternating sheets, each containing only molecules of identical stereochemistry, and the all-*syn* and all-*anti* chains from adjacent sheets are perpendicular to each other. Similar to **4-HOBDI**,[6] the double bonds in the crystals of **3-HOBDI**, **2-FBDI**, and **2,5-DMBDI** are separated at distances <4 Å, but only in form C of **3-HOBDI**, **2,5-DMBI**, and **3-MOBDI** are they entirely parallel to each other (Figure 4 and Table 1).

2.4. Steady-State and Time-Resolved Spectroscopy of BDIs. To examine whether the emission properties of the solid-state BDI chromophores were stacking-mode specific, which might have implications for the GFP photochemistry, we used our previous approach,[6] where we correlated the spectral features of **4-HOBDI** and its ethers in the solid-state with their crystal packing properties, leading to fine-tuning of monomer−excimer emission. The two-dimensional excitation−emission spectra recorded from solid sample of **3-HOBDI**-A are shown in Figure 5. The variety of offset stacking geometries that we observe here for different substituents (Figure 4) provides grounds for

(14) (a) Bernstein, J. *Polymorphism in Molecular Crystals*; Oxford University Press: Oxford, 2002; pp 170−176. (b) Price, C. P.; Grzesiak, A. L.; Matzger, A. J. *J. Am. Chem. Soc.* **2005**, *127*, 5512–5517. (c) Chen, S.; Guzei, I. A.; Yu, L. *J. Am. Chem. Soc.* **2005**, *127*, 9881–9885. (d) Chen, S.; Xi, H.; Yu, L. *J. Am. Chem. Soc.* **2005**, *127*, 17439–17444.

Table 1. Selected Structural and Spectroscopic Parameters of the Benzylidenedimethylimidazolinones (BDIs)

	structural parameters			spectral parameters				
cmpd	*d*/Å	bond parallelism	reactivity	λ_{max}^{abs} (DMSO)[a]	λ_{max}^{em} (DMSO)[a]	λ_{max}^{ex} (solid)[a]	λ_{max}^{em} (solid)[a]	τ
2-MeBDI	6.892	Y	N	363	429	395	440	0.99 ns (445 nm)
3-HOBDI-A	3.649, 3.555	N	Y	366	436	390	440	ultrafast (440 nm)
	4.005, 4.176	N						100 ps (DMSO)
3-HOBDI-B	3.871, 3.556	N	Y			–	–	–
3-HOBDI-C	3.574	Y	Y			–	–	–
	4.299	Y						
2-FBDI	3.848	Y	Y	363	433	390	459, 570	ultrafast (450 nm)
	3.716	Y				450	500	2.7 ns
								73 ps (DMSO)
3-MOBDI	6.964	Y	N	365	432	?	450	130 ps
							520	1.5 ns, 10.6 ns (biexp.)
								40 ps (DMSO)
2,5-DMBDI	3.783	Y	Y	368	429	?	450	ultrafast (450 nm)
	5.483	Y					~550	1.56 ns, 3.56 ns (biexp.)
2,4-DMBDI	4.078, 4.526	Y	N	366	429	430	470	1.0 ns, 4.1 ns (biexp.)
4-HOBDI	3.705, 3.585	N	Y					ultrafast (440 nm)

[a] In nanometers.

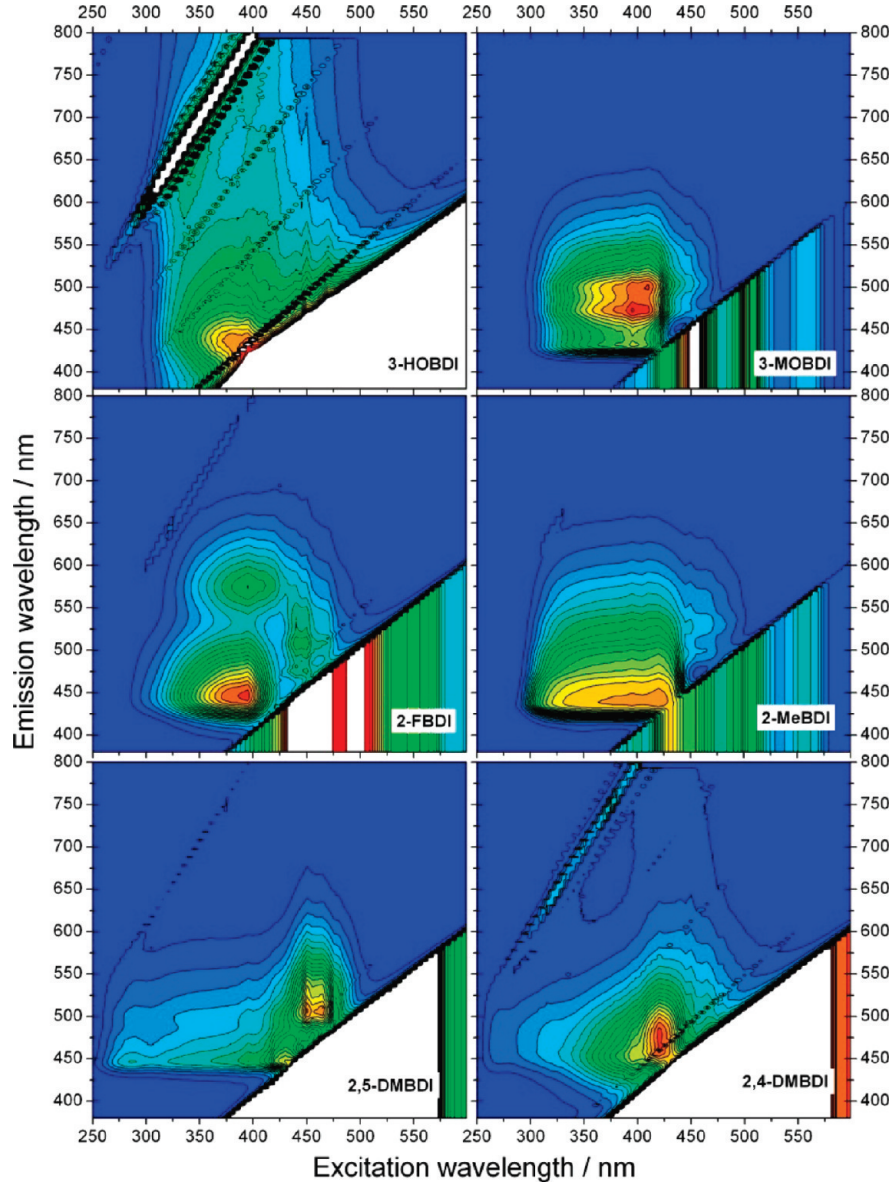

Figure 5. Excitation−emission contour profiles of the solid GFP model chromophores. The intensity increased from blue to red regions.

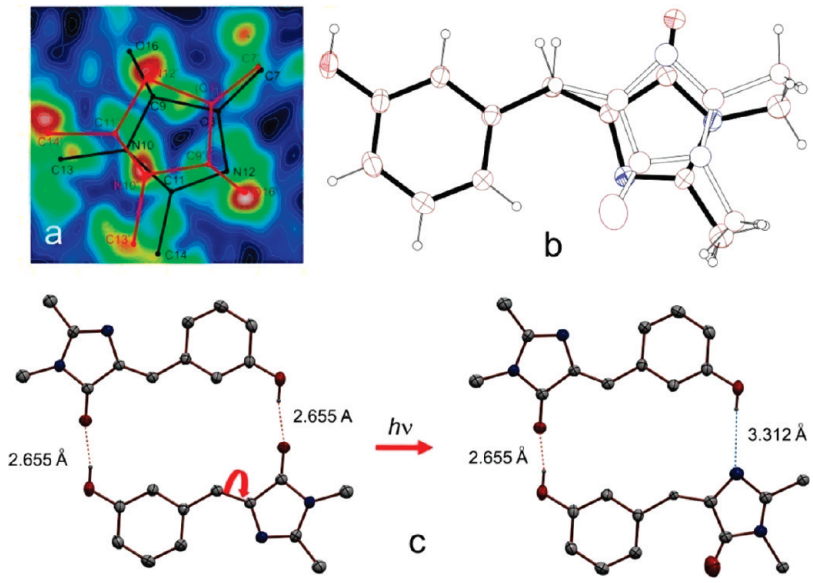

Figure 6. (a) Slice of the residual electron density ($F_{obs} - F_{calc}$) through the imidazolinone half of the major (unreacted) component molecule in a crystal of **3-HOBDI**-C that was exposed to room light during several weeks. The electron density increases from deep blue (negative) to white (positive) regions. The parent (*Z*-**3-HOBDI**) and product conformations (*E*-**3-HOBDI**) are represented as black and red sticks, respectively. Note that the structure of *E*-**3-HOBDI** is drawn through the *projections* of the observed maximum peaks onto the ring plane of *Z*-**3-HOBDI**, which appears as offset of the difference peak maxima from the atomic positions of *E*-**3-HOBDI**. (b) ORTEP-style plot of the disordered molecule of **3-HOBDI** in the crystals of form C exposed to visible light. The major (*Z*-**3-HOBDI**, 87.1%) and minor (*E*-**3-HOBDI**, 12.9%) components are represented as full and empty ellipsoids/bonds, respectively. (c) Changes in the hydrogen-bonding pattern occurring upon single τ one-bond flip in the dimers of **3-HOBDI**-C and respective O···O or O···N distances. All but the hydroxyl hydrogen atoms are omitted for clarity. The hydrogen-bonded dimers in the unreacted crystal (left) and in the reacted crystal (one molecule in *Z*-**3-HOBDI** conformation and the other in *E*-**3-HOBDI** conformation, right) are shown.

more quantitative consideration of the relative importance of aggregation- and stacking-induced modulation of the emission energy.

In polar aprotic solvent (DMSO)[15] all six compounds demonstrated amazingly similar absorption and emission spectra (Figure S9 in the SI), showing very weak spectral dependence on the nature of the phenyl ring substituents. Minor bathochromic shifts of **3-HOBDI** emission maxima and broadening of the spectrum can be explained by the known solvatochromic behavior of phenols in basic solvents.[16] The fluorescence decays of **2-MeBDI**, **2,4-DMBDI** and **2,5-DMBDI** were faster than 10 ps, the time resolution of our TCSPC instrument. However, the fluorescence lifetimes of **3-MOBDI**, **2-FBDI** and **3-HOBDI** were considerably longer (as reported earlier for the latter compound),[17] and therefore they could be measured using TCSPC. Spectral and kinetic data of all compounds are summarized in Table 1.

2.5. X-ray Photodiffraction Analysis of 3-HOBDI-C. During handling of the BDI crystals, we noticed that some of the crystals which had not been protected from the fluorescent room light, gradually turned opaque during period of several weeks, even without prior exposure to UV light. Most of the samples developed visible cracks perpendicular to their longest axis, and some also became curved (for micrographs of the curved crystals of **2-FBDI**, see Figure S10 in the SI). Intrigued by the reason for the apparent sensitivity of the BDI samples to visible light, we approached X-ray diffraction analysis of the opaque crystals which had been stored in air at room light for several weeks, performing all further experimental procedures (including the diffraction data collection) under red safelight ($\lambda > 660$ nm). The reacted crystals from most of the samples were of insufficient diffraction quality, due to partial disintegration and/or deformation. Only in the case of **3-HOBDI**-C, for which the crystal shape remained the least deformed, could we succeed in selecting several well-diffracting opaque specimens which remained compact for analysis with X-ray diffraction.

The X-ray photodiffraction analysis of a reacted **3-HOBDI**-C crystal, where the **3-HOBDI** molecule is in its *Z* configuration (*Z*-**3-HOBDI**), revealed that the crystal symmetry was preserved. However, the difference Fourier electron density map ($F_{obs} - F_{calc}$) clearly showed new peaks around the imidazolone ring from a secondary, product species with a population that refined to 12.9% (Figure 6a).[18] In the structure of the crystal refined as a two-component mixture,[19] the carbonyl group of the product, which due to the symmetric methyl substitution represented a useful marker of the orientation of the imidazolone ring, was flipped to the opposite side of the ring relative to the

(15) The absorption and emission spectra of **3-HOBDI** and **3-MOBDI** in various solvents have been reported earlier (see ref 1c).

(16) (a) Solntsev, K. M.; Huppert, D.; Tolbert, L. M.; Agmon, N. *J. Am. Chem. Soc.* **1998**, *120*, 7981–7982. (b) Solntsev, K. M.; Huppert, D.; Agmon, N. *J. Phys. Chem. A* **1998**, *102*, 9599–9606. (c) Dong, J.; Solntsev, K. M.; Tolbert, L. M. *J. Am. Chem. Soc.* **2006**, *128*, 12038–12039.

(17) Dong, J.; Solntsev, K. M.; Poizat, O.; Tolbert, L. M. *J. Am. Chem. Soc.* **2007**, *129*, 10084–10085.

(18) All atoms except for C3′ of the imidazolone ring of the product molecule (primed in Figure 7) were clearly observed in the difference map. The secondary component of the *ipso*-carbon (C3′) could not be observed as sufficiently high separate residual density, probably due to its close proximity with the same atom (C3) of the reactant. Within the molecule, residual peaks of only the imidazolone ring and the bridging C-atom were observed, showing that the molecular isomerization occurs only on the imidazolone half of the molecule; the position of the phenyl ring did not change during the reaction, and therefore, it was refined as a single component.

(19) **3-HOBDI**-C (after exposure to visible light; CCDC 61987): $C_{12}H_{12}N_2O_2$, $M_r = 216.24$, triclinic, $P\bar{1}$, $Z = 2$, $a = 7.0622(4)$ Å, $b = 7.2019(4)$ Å, $c = 11.5013(6)$ Å, $\alpha = 73.718(3)°$, $\beta = 80.875(3)°$, $\gamma = 75.073(2)°$, $V = 540.20(5)$ Å^3, data/restraints/parameters: 2470/9/165, GoF = 1.018, $R_1 = 8.06\%$.

double bond (Figure 6b). The residual peaks corresponding to the methyl groups and the nitrogen atoms were also significantly and simultaneously shifted, so that the imidazolone ring of the product represented slightly offset mirror image of that of the reactant, which appeared as an increased angle at the bridging carbon atom. Except for somewhat increased thermal ellipsoids, no significant movements could be detected for the phenyl carbon atoms, so that the phenyl ring was retained at nearly identical position as in the reactant. It should be noted that the product molecule, with the τ-flipped imidazolone ring and E configuration (*E*-**3-HOBDI**), was the only detectable product; particularly, no evidence of a dimeric product (that is, peaks corresponding to cyclobutane atoms)[12] could be observed. This result clearly showed that the τ-one-bond-flipped isomer *E*-**3-HOBDI** was the main product of this slow photoreaction in the crystal exposed to visible light.

3. Discussion

3.1. General. Spatial and temporal *in vivo* monitoring of the GFP-tagged proteins, for example, by the double-labeling FRET method,[20] requires excitation of the chromophore. The wild-type GFP absorbs at 397 nm (A band) and 475 nm (B band), corresponding to the neutral molecule and the conjugate base of the emitter, respectively, and excitation of both bands results in the green emission of the ion at 508 nm. Low-energy excitation with light of moderate power induced reversible changes and isomerization of the protein structure via a Förster cycle.[21] However, at higher energies and increased light density, complex reactions leading to irreversible changes of the protein structures may occur, typically, decarboxylation of the proximate glutamate residue.[22] Such denaturation processes can be important for analytical methods which require high input powers due to low signal for detection, such as single-molecule spectroscopy[23] or fluorescence correlation spectroscopy.[24] The primary processes triggering irreversible chemical reactions of the protein are believed to start at the chromophore itself, and thus complete understanding of the photochemistry from the higher-order transitions and the faith of low-energy excitations which do not contribute to the main reaction pathways is essential to the improvement of the analytical feasibility of the GFP-like proteins. Such irreversible processes in model GFP systems and, particularly, the allosteric-like response from the chromophore environment, however, have not been investigated yet.

By having access to a large variety of chromophores of similar electronic structure but varied crystal packing, we have a unique opportunity to examine how crystal packing influences their varied behavior, from photophysics to photodimerization to photoisomerization. On the one hand, the presence of a double bond in close proximity to another leads to efficient cycloaddition, a phenomenon that has been extensively studied in the cinnamate literature.[25] When such proximity is accompanied by an extensive hydrogen-bonded network, the bond contraction produced by dimerization can lead to a surprising photomechanical effect. On the other hand, when such proximity is absent, dimerization is extinguished, and isomerization can take place. We now consider each of these phenomena in turn.

3.2. Effect of Crystal Packing on the Emission Spectra of BDIs. We find that the crystal packing of the BDIs strongly affects their fluorescence properties in the solid state, and it is reproduced well in the two-dimensional excitation−emission spectra (Figure 5). In the crystal of **2-MeBDI**, where the molecules are offset and isolated from each other (the distance between the double bonds is 6.892 Å) and they interact only by weak C−H···O hydrogen bonds (d(C···O) = 3.425 Å), the excitation energy remains localized within individual molecules. The emission from the singlet excited state, with $\lambda_{max}^{ex} = 395$ nm, appears as a single strong peak with $\lambda_{max}^{em} = 440$ nm, along with the existence of a single major emitting species. As reported previously,[6] this band is slightly red-shifted by the environmental effects relative to the emission in solution (431 nm). The decay times are weakly dependent on the wavelength and range from 0.99 ns (445 nm) to 1.37 ns (490 nm). Contrary to the isolated emission observed from **2-MeBDI**, in the structure of **3-HOBDI**-A, where the molecules exist as hydrogen-bonded chains (d(O−H···O)$_{syn-syn}$ = 2.754 Å, d(O−H···O)$_{anti-anti}$ = 2.682 Å), the cooperative effects from the intermolecular interactions are expected to affect significantly the emission intensity and the time-decay profile from the individual molecules. Accordingly, only a weak emission with one major emission peak with $\lambda_{max}^{ex} = 390$ nm and $\lambda_{max}^{em} = 440$ nm is observed. At all wavelengths, the decays of the emission are non-monoexponential and ultrafast, the major amplitude with a contribution of >98% weight corresponding to a species that decays within 10 ps, which remains below the detection limit. Similar efficient fluorescence quenching in the solid state was observed previously for **4-HOBDI**.[6]

In collaboration with Seth Olsen we propose a possible mechanism of **3-HOBDI** fluorescence quenching in the solid state. A full description of the mechanism is given in the Supporting Information. Briefly, our hypothesis describes the photochemistry of **3-HOBDI** (as well as **4-HOBDI**) within a model space spanned by three frontier orbitals localized on the rings and bridge.[26,27] Within such a model, it has been shown[28] that changing the protonation state of one of the rings at its oxygen changes the local frontier energy (i.e., the Brooker basicity[29,30]) on a scale comparable to that of the resonance interaction between the rings (i.e., the isoenergetic excitation of the asymmetric dye, given as the harmonic mean of the excitation energies of the parent symmetric dyes[29,30]). These arguments do suggest that quenching by proton transfer may occur when **HOBDI** *changes its net titration state*. Such a mechanism is outlined in Figure S11 (SI). Within this mechanism, only *one of each pair* of **HOBDI** molecules transfers its phenolic proton to the imidazolinone carbonyl of its hydrogen bond-accepting partner. This is equivalent to displacement along

(20) Lippincott-Schwartz, J.; Snapp, E.; Kenworthy, A. *Nat. Rev. Mol. Cell Biol.* **2001**, *2*, 444–456.
(21) Brejc, K.; Sixma, T. K.; Kitts, P. A.; Kain, S. R.; Tsien, R. Y.; Ormö, M.; Remington, S. J. *Proc. Natl. Acad. Sci. U.S.A.* **1997**, *94*, 2306–2311.
(22) (a) van Thor, J. J.; Gensch, T.; Hellingwerf, K. J.; Johnson, L. N. *Nat. Struct. Biol.* **2002**, *9*, 37–41. (b) Bell, A. F.; Stoner-Ma, D.; Wachter, R. M.; Tonge, P. J. *J. Am. Chem. Soc.* **2003**, *125*, 6919–6926.
(23) Dickson, R. M.; Cubitt, A. B.; Tsien, R. Y.; Moerner, W. E. *Nature* **1997**, *388*, 355–358.
(24) Haupts, U.; Maiti, S.; Schwille, P.; Webb, W. W. *Proc. Natl. Acad. Sci. U.S.A.* **1998**, *95*, 13573–13578.
(25) (a) Lewis, F. D.; Quillen, S. L.; Hale, P. D.; Oxman, J. D. *J. Am. Chem. Soc.* **1988**, *110*, 1261–1267. (b) Bertmer, M.; Nieuwendaal, R. C.; Barnes, A. B.; Hayes, S. E. *J. Phys. Chem. B* **2006**, *110*, 6270–6273.
(26) Olsen, S.; McKenzie, R. H. *J. Chem. Phys.* **2009**, *130*, 184302.
(27) Olsen, S.; McKenzie, R. H. *J. Chem. Phys.* **2009**, *131*, 234306.
(28) Olsen, S. *J. Chem. Theory Comput.* **2010**, DOI: 10.1021/ct100001b.
(29) Platt, J. R. *J. Chem. Phys.* **1956**, *25*, 80–105.
(30) Brooker, L. G. S. *Rev. Mod. Phys.* **1942**, *14*, 275–298.

a *nonuniform* proton transport coordinate and generates ion pairs consisting of (deprotonated) anion and (diprotonated) cationic **HOBDI** species, as shown. The energy gap between HOMO and LUMO frontier orbitals for the anion and cation should be comparable, by the arguments above. However, the orbital energies will be shifted in opposite directions by the net charge on each of the ions, by an amount that is significant on the scale of the HOMO−LUMO splitting. The frontier orbitals of the anion are shifted up, while those of the cation are shifted down. This places the empty LUMO of the cation between the singly occupied HOMO and LUMO of the anion. Such an arrangement—with the LUMO of one species in between the HOMO and LUMO of another—is a common motif in electron transfer quenching mechanisms.[31]

Although each of **2-FBDI** and **3-MOBDI** contains a single structural type of the respective molecule, they exhibit at least two emission centers, which are separated better in the case of **2-FBDI**. For **2-FBDI**, the stronger emitter is excited at $\lambda_{max}^{ex} = 390$ nm and emits at two wavelengths, $\lambda_{max,1}^{em} = 450$ nm and $\lambda_{max,1}^{em} = 570$ nm. The second emitter, excited at $\lambda_{max}^{ex} = 450$ nm, exhibits wider energy distribution and emits at $\lambda_{max,1}^{em} = 500$ nm. At 595 nm, the lifetime of the second component is 2.7 ns. The two emissions of **3-MOBDI** are strongly overlapped. The species emitting at $\lambda_{max,1}^{em} = 450$ nm decays at 130 ps, while the one $\lambda_{max,1}^{em} = 500$ nm, with rise time of 240 ps, follows a biexponential decay law, with component lifetimes of 1.5 and 10.6 ns and an amplitude ratio of 12:1. Unlike **2-MeBDI** and **3-HOBDI**, the molecules of **2-FBDI** and **3-MOBDI** are not completely isolated, and they are not characterized by extensive hydrogen bonding. Instead, in both cases two molecules are stacked with each other with at least one-half of their skeleton (Figure 4). **2-FBDI** forms antiparallel dimers, where both the phenyl and the imidazolone rings of one molecule are stacked with the imidazolone and phenyl ring from its molecular counterpart. In the structure of **3-MOBDI**, the molecules are displaced relative to each other, so that only one-half of the molecule forms stack with the neighbor molecule (that is, the phenyl ring is stacked with an imidazolone ring). The emission of the individual molecules in such case will be affected by the proximity of the molecules by activation of excimer transitions, which could explain the complicated pattern observed in the kinetics of their emission spectra.

3.3. Photomechanical Effects in Crystalline BDIs. Mechanical effects in photomechanically active materials[32] and thermosalient crystals[33] (the latter occasionally also referred to as "jumping crystals"), such as the one described here for **3-HOBDI**, are extremely rare solid-state phenomena and are considered important for the design of actuators, as well as for conversion of the light or kinetic energy into mechanical work. In particular, photomechanical effects in the solid state present an opportunity for photoactuators in several photoactive systems. A large number of these have relied upon *cis*/*trans* isomerization of azobenzene as the structural perturbation, with a clever recent example.[32c] More commonly, such effects have been developed for azobenzene-containing polymers,[34] although examples using [2 + 2][35] and [4 + 4][32a,b] cycloadditions have also been reported. **3-HOBDI-**A presents a startling example for which a unique polymorph presents a special deactivation pathway.

The very low excitation power, uniform excitation of the crystal, high melting point, short exposure time and absence of photomechanical effects in the other compounds (even when the crystal shape is similar to that of **3-HOBDI**-A, such as is the case with **2-FBDI**) all indicate that the photoinduced effects observed for **3-HOBDI**-A are not due to heating or partial (surface) melting but to the photochemical reaction which was evidenced by IR (Figures S1−S6 in the SI) and NMR spectroscopy (Figure 2) for bulk samples. The two-dimensional excitation−emission profiles (Figure 5) show that, in contrast to the other compounds, the fluorescence of **3-HOBDI** is quenched in the solid state. This observation may indicate deexcitation through nonradiative pathways due to strong intermolecular interactions (hydrogen bonding) or by means of photochemical reaction from the excited state.

The main reason behind the different photochemical properties and the appearance of dramatic photomechanical effects of **3-HOBDI**-A, which are not observed for the other forms of **3-HOBDI** and the other compounds in this group, are the strongly anisotropic packing interactions. As explained above, the structure of **3-HOBDI**-A is composed of layered two-dimensional sheets of all-*syn* hydrogen-bonded strings parallel to the *c*-axis and alternating and perpendicular to each other, with all-*anti* zigzag strings parallel to the *b*-axis (see Chart 2 and Figure 7a). Larger bunches of the coaxial molecular strings in **3-HOBDI**-A are observed by AFM spectroscopy as ridges in the surface of nonirradiated crystal (Figure 7b). The surface of the crystal is relatively smooth with a roughness of 2.6−6.4 nm. From these dimensions, the surface of the crystal appears fluted, reminiscent of a grating, with large ridges approximately 1 μm apart. Individual structures consist of smaller, parallel string substructures, with some layering close to the top of the features also being apparent. This arrangement is reminiscent of cylinders placed side-by-side. The molecules within the chains are held together by strong intermolecular O−H···O hydrogen bonds, whereas the stacked sheets are crisscrossed and interact with each other through weak $\pi-\pi$ interactions. Unlike forms

(31) Klessinger, M.; Michl, J. *Excited States and Photochemistry of Organic Molecules*; VCH Publishers, Inc.: New York, 1995; p 283.

(32) Selected examples: (a) Al-Kaysi, R. O.; Müller, A. M.; Bardeen, C. J. *J. Am. Chem. Soc.* **2006**, *128*, 15938–15939. (b) Al-Kaysi, R. O.; Bardeen, C. J. *Adv. Mater.* **2007**, *19*, 1276–1280. (c) Koshima, H.; Ojima, N.; Uchimoto, H. *J. Am. Chem. Soc.* **2009**, *131*, 6890–6891. (d) Barrett, C. J.; Mamiya, J.; Yager, K. G.; Ikeda, T. *Soft Matter* **2007**, *3*, 1249–1261. (e) Colombier, I.; Spagnoli, S.; Corval, A.; Baldeck, P. L.; Giraud, M.; Léaustic, A.; Yu, P. *Mol. Cryst. Liq. Cryst.* **2005**, *431*, 495–499. (f) Bubnov, M. P.; Nevodchikov, V. I.; Fukin, G. K.; Cherkasov, V. K.; Abakumov, G. A. *Inorg. Chem. Commun.* **2007**, *10*, 989–992. (g) Yamada, M.; Kondo, M.; Mamiya, J.; Yu, Y.; Kinoshita, M.; Barrett, C. J.; Ikeda, T. *Angew. Chem., Int. Ed.* **2008**, *47*, 4986–4988. (h) Kobatake, S.; Takami, S.; Muto, H.; Ishikawa, T.; Irie, M. *Nature* **2007**, *446*, 778–781.

(33) (a) Zamir, S.; Bernstein, J.; Greenwood, D. J. *Mol. Cryst. Liq. Cryst.* **1994**, *242*, 193–200. (b) Steiner, T.; Hinrichs, W.; Saenger, W. *Acta Crystallogr.* **1993**, *B49*, 708–718. (c) Kaftory, M.; Botoshansky, M.; Kapon, M.; Shteiman, V. *Acta Crystallogr.* **2001**, *B57*, 791–799. (d) Lieberman, H. F.; Davey, R. J.; Newsham, D. M. T. *Chem. Mater.* **2000**, *12*, 490–494. (e) Crottaz, O.; Kubel, F.; Schmid, H. *J. Mater. Chem.* **1997**, *7*, 143–146. (f) Corbett, J. M.; Dickman, M. H. *Acta Crystallogr.* **1996**, *C52*, 1851–1853. (g) Ding, J.; Herbst, R.; Praefcke, K.; Kohne, B.; Saenger, W. *Acta Crystallogr.* **1991**, *B47*, 739–742. (h) Gigg, J.; Gigg, R.; Payne, S.; Conant, R. *J. Chem. Soc., Perkin Trans. I* **1987**, 2411–2414. For remarkable recent studies of mechanical properties of molecular crystals, see: (i) Reddy, C. M.; Gundakaram, R. C.; Basavoju, S.; Kirchner, M. T.; Padmanabhan, K. A.; Desiraju, G. R. *Chem. Commun.* **2005**, 3945–3947. (j) Reddy, C. M.; Kirchner, M. T.; Gundakaram, R. C.; Padmanabhan, K. A.; Desiraju, G. R. *Chem.—Eur. J.* **2006**, *12*, 2222–2234. (k) Reddy, C. M.; Basavoju, S.; Desiraju, G. R. *Chem. Commun.* **2005**, 2439–2441.

(34) Zhang, C.; Zhao, X.; Chao, D.; Lu, X.; Chen, C.; Wang, C.; Zhang, W. *J. Appl. Polym. Sci.* **2009**, *113*, 1330–1334.

(35) (a) He, J.; Zhao, Y.; Zhao, Y. *Soft Matter* **2009**, *5*, 308–310. (b) Lendlein, A.; Jiang, H.; Juenger, O.; Langer, R. *Nature (London)* **2005**, *434*, 879–882.

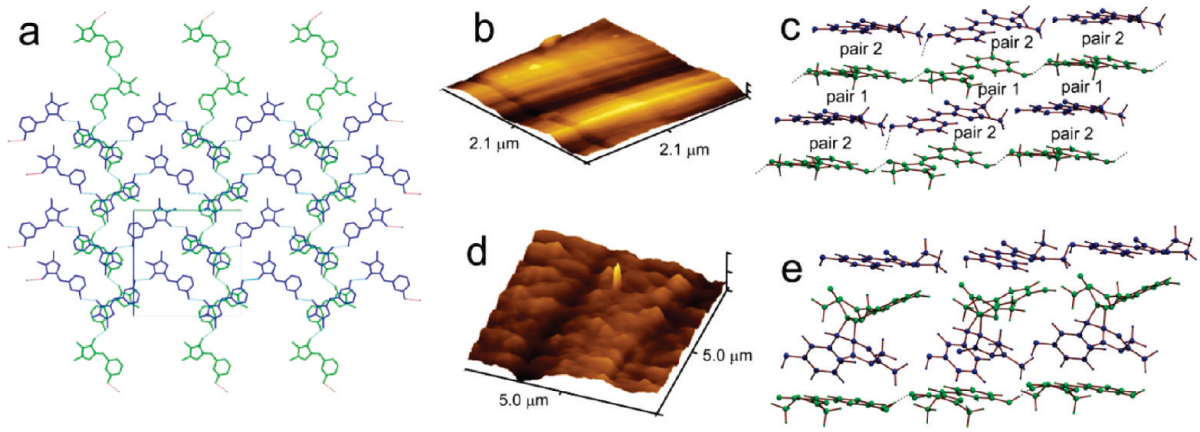

Figure 7. (a) Sheets of hydrogen-bonded chains of *syn* (green) and *anti* (blue) **3-HOBDI** molecules in the crystal of **3-HOBDI**-A. (b) and (d): AFM images of the crystal surface before and after UV irradiation, showing the UV-induced changes of the crystal surface morphology. (c) and (e): Packing of the crisscrossed layers of *syn*-**3-HOBDI** (green) and *anti*-**3-HOBDI** (blue) in the unreacted crystal (c) and in a model structure in which the closer pairs are dimerized, considering the usual geometry of the central cyclobutane ring.

Chart 2. Polymeric (a, b) and Dimeric (c) Hydrogen-Bonding Patterns Observed in the Three Characterized[11] Polymorphs of **3-HOBDI**

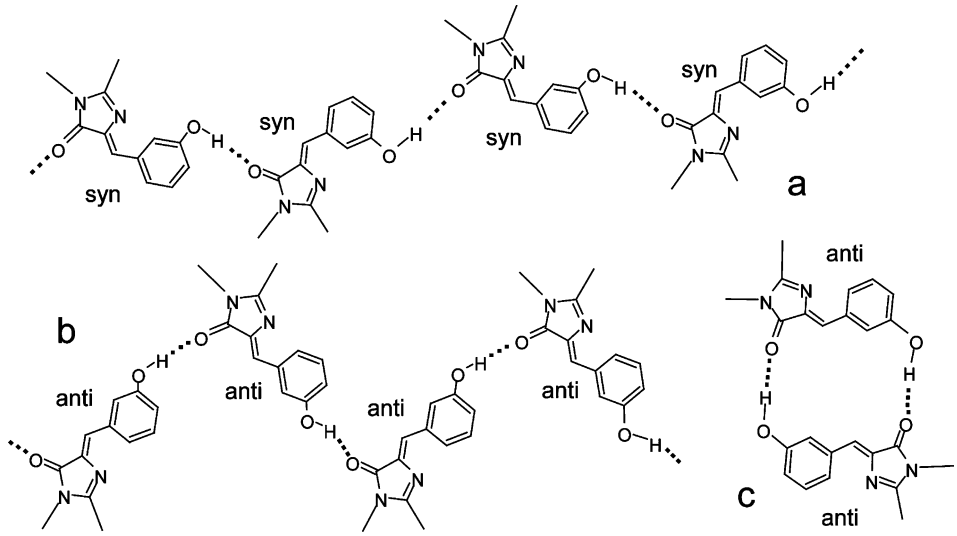

B and C, for which the strong interactions in the crystal are confined within the doubly hydrogen-bonded head-to-tail *anti* dimers (Chart 2), the infinite chains of strong hydrogen bonds in **3-HOBDI**-A provide notable strength and flexibility within the sheets and could act as the basis for one-dimensional transfer of cooperative effects within the crystal. Being glued by much weaker interactions, the shear-free, individual sheets have greater freedom to slide over the top of each other, which is related to the unusual elasticity of the crystals of form A during the bending.

Pairs of any two symmetrically nonequivalent molecules from the adjacent perpendicular strings (colored green and blue in Figure 7a), which are stacked in antiparallel displaced fashion, define two types of alternating C---C separations, with nearly identical interbond dihedrals: molecular pair 1 (3.648 and 3.555 Å, angle: 56.9°) and molecular pair 2 (4.005 and 4.176 Å, angle 57.3°). According to the topochemical criteria,[12] it is expected that all bonds of the first, closer pair, are photoreactive. Although there might be competition for dimerization between the two pairs, the notable difference in the double bond separations at virtually identical relative orientations of the double bonds indicates that the dimerization of the double bonds within the pair of closer bonds (bond pair 1) is preferred and largely prevents subsequent reaction between the bonds of the more distant moieties (bond pair 2). Coincidentally, such dimerization leads to a *trans,trans* symmetric dimer which is the most stable according to semiempirical calculations. Therefore, most of the molecules from one sheet selectively form dimers with their counterpart molecules from the other sheet rather than from different sheets; that is, the dimers are almost exclusively formed between molecular pairs 1 but not between molecular pairs 2, as shown in c and e of Figure 7. Due to the bending of the individual reacting molecules and the inclination of the phenyl rings upon the cyclobutane ring formation, the molecules of the dimerized sheets become devoid of the π—π interactions with molecules from the adjacent dimerized (or still monomeric) sheets, thus resulting in "pairing" of the originally equidistant sheets and subsequent separation of the resulting sheet pairs. The disappearance of the π—π interactions, which served as weak "glue" between the paired sheets, increases their mobility in respect to each other, so that small perturbations such as local heating or defects are expected to cause significant and cooperative sliding of the sheets of dimers relative to each other. This photomechanical effect, which is macroscopically observed as bending of **3-HOBDI**-A crystals, is induced by dimerization, and it is shear-driven at a molecular level. Moreover, because

the original strings are composed of different types of molecules (*syn* and *anti* along the *c*- and *b*-axes, respectively), the preferences for sliding along each of the two directions are different, which corresponds well with the subsequent bending along the second-longest axis that ultimately results in a twisting motion. Apparently, after maximum strain has been achieved by sliding of the paired layers in one direction, the sliding in the second direction becomes dominant to the point where the mechanical strain overweighs the cooperative forces, and a macroscopic crack appears on the crystal perpendicular to its longest axis (Figure 1h, Movie S1 (SI)). This mechanism is consistent with the absence of observable photomechanical effect in forms **3-HOBDI**-B and **3-HOBDI**-C, where the *anti* molecules form head-to-tail bonded dimers (Chart 2), despite the fact that both forms are photochemically active (IR spectroscopy). Although the dimerization in forms B and C occurs, the crystals do not bend, but instead they tend to crack normal to the longest axis. Similar disintegration is observed for the other photoreactive compounds (**2-FBDI** and **2,5-DMBDI**).

As exemplified with the *syn* chains in the mechanism shown in Figure 7e, the formation of dimers inevitably results in disruption of the intermolecular hydrogen bonds by separation of the hydroxyl (donor) and keto (acceptor) groups from each other, which is confirmed by the large blue-shift (125 cm^{-1}) of the ν(OH) mode observed in the IR spectra of the completely photoreacted sample (Figure S2 in the SI). The disruption of the hydrogen bonds along the strings and the notable shrinkage of the strings due to the bending of the component molecules (Figure 7e) are expected to result in accumulation of mechanical stress along the strings. On a microscopic scale, this perturbation of large numbers of molecules along the initially straight strings has to be released, which would affect the macroscopic appearance of the crystal surface. Indeed, AFM images of UV-irradiated crystal (Figure 7d) show that the crystal surface is visibly more disturbed, and the roughness has increased to 10−14 nm. The initially smooth parallel "waves" appear "chopped" and out-of-plane, giving the crystal surface a fish-scale appearance—a consequence of crystal bending and mass redistribution. The image of the crystal which remained unattached to the basis is similar, but the roughness, depending on area, is as low as 7 nm but as high as 43 nm.

3.4. Packing Effects on the Photoisomerization by One-Bond Flip. In contrast to **3-HOBDI**-A, **3-HOBDI**-C allows us to test the influence of crystal packing on *cis*/*trans* isomerization. The hula twist has been accepted as a compelling rationale for chromophore isomerization in fluorescent proteins.[36] Nevertheless, considerable theoretical[37] and experimental[38] evidence exists that such a double motion pays considerable energetic penalties within the fluorescent protein barrel. Unfortunately, neither tyrosine nor phenylalanine, both of which form the aromatic rings of the largest group of protein chromophores, has a *meta* or *ortho* substituent to isolate the double twist. Either the tryptophan or histidine derivative ("cyan fluorescent protein") could plausibly test such motions.

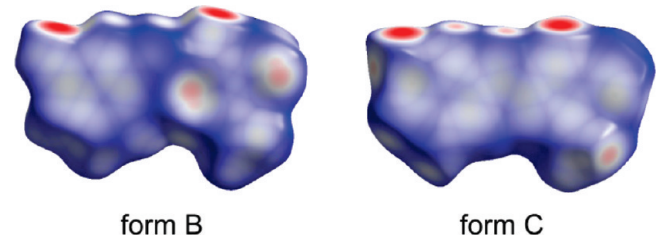

Figure 8. Hirshfeld surfaces[40] (plotted as d_{norm}) of the molecules in forms B and C of **3-HOBDI**.

Although the relevance of our observations to the protein itself can be argued, we note that when the aromatic ring is constrained by hydrogen bonding as in **3-HOBDI**-C, facile isomerization via one-bond rotation about the double bond occurs even within the solid state (Figure 6). From the X-ray diffraction analysis of partially photoreacted crystal, it is concluded that, while dimers of the BDIs are obtained by high-energy excitation (365 nm; see the NMR, IR and MS results described above), in single crystals of **3-HOBDI**-C, prolonged exposure to low excitation energies in the visible region (ambient light) cause $Z-E$ isomerization with a τ one-bond flip of the imidazolone ring. Similar dependence on the dimerization versus isomerization on the excitation energy was reported previously for solutions of 5-aryl- and 5-pyridylmethylenehydantoins.[39] Our result represents the first direct evidence of such processes occurring in crystals of pure BDI chromophore. On the basis of this observation, we conclude that conservation of volume is not a sufficient impediment to isomerization via a bond twist.

Closer analysis of the supramolecular structure in the **3-HOBDI**-C crystal reveals an important effect of the photoreaction, induced from the excited state, to the intermolecular interactions. Assuming a statistical distribution of the product molecules, the small conversion (12.9%) implies that, after imidazolone ring flipping, almost every reactive molecule rebinds to its nonreacted counterpart (Figure 6c). Therefore, because the position of the phenyl half of the molecule is essentially preserved in the product, a weaker hydrogen bond O−H···N (3.312 Å) is substituted for a stronger hydrogen bond O−H···O (2.655 Å). This clearly thermodynamically disfavored process is only possible from an excited state. Once created, however, the flipped product is stabilized by the newly formed hydrogen bond, which is why the product molecule accumulates in detectable amounts. This result may have implications for the one-bond flip mechanism suggested for the GFP chromophore.

The dimers in **3-HOBDI**-B and **3-HOBDI**-C are confined to a space of similar shape, and the two molecules within each dimer interact with hydrogen bonds of similar strength. Yet only in the latter can flipping occur to a significant extent without interfering with the long-range crystalline order. This observation can be rationalized by inspection of the Hirshfeld surfaces[40] plotted around the respective monomers (Figure 8). The Hirshfeld surfaces[41−44] provide a convenient way to depict the

(36) (a) Maddalo, S. L.; Zimmer, M. *Photochem. Photobiol.* **2006**, *82*, 367–372. (b) Megley, C. M.; Dickson, L. A.; Maddalo, S. L.; Chandler, G. J.; Zimmer, M. *J. Phys. Chem. B* **2009**, *113*, 302–308.
(37) (a) Norton, J. E.; Houk, K. N. *Mol. Phys.* **2006**, *104*, 993–1008. (b) Martin, M. E.; Negri, F.; Olivucci, M. *J. Am. Chem. Soc.* **2004**, *126*, 5452–5464.
(38) (a) Saltiel, J.; Bremer, M. A.; Laohhasurayotin, S.; Krishna, T. S. R. *Angew. Chem., Int. Ed.* **2008**, *47*, 1237–1240. (b) Saltiel, J.; Krishna, T. S. R.; Turek, A. M. *J. Am. Chem. Soc.* **2005**, *127*, 6938–6939.
(39) Tan, S.-F.; Ang, K.-P.; How, G.-F. *J. Phys. Org. Chem.* **1991**, *4*, 707–713.
(40) Hirshfeld, F. L. *Theor. Chim. Acta* **1977**, *44*, 129–138.
(41) McKinnon, J. J.; Spackman, M. A. *Chem. Commun.* **2007**, 3814–3816.
(42) McKinnon, J. J.; Mitchell, A. S.; Spackman, M. A. *Chem.—Eur. J.* **1998**, *4*, 2136–2141.
(43) McKinnon, J. J.; Spackman, M. A.; Mitchell, A. S. *Acta Crystallogr.* **2004**, *B60*, 627–668.
(44) Wolff, S. K.; Grimwood, D. J.; McKinnon, J. J.; Jayatilaka, D.; Spackman, M. A. *CrystalExplorer*; University of Western Australia: Perth, Australia, 2007.

molecular shape and to visualize the intermolecular interactions. They represent plots, which are obtained by partitioning the space in the crystal into regions where the contribution from the electron distribution of a sum of spherical atoms for the molecule exceeds the contribution from the corresponding sum over the crystal. From the red regions on the imidazolone ring in **3-HOBDI**-B it becomes apparent that it is sandwiched more tightly and interacts more strongly by the surrounding neighbor molecules. The imidazolone ring in **3-HOBDI**-C, on the other hand, interacts weakly and thus has larger freedom for flipping.

4. Conclusions

It has been common practice to consider the reactivity of molecules independent of their extended environment. With the advent of "supramolecular photochemistry", we now recognize that reactivity can be promoted or constrained by rigid environments. The systems studied here illustrate that when the "solvent" is the molecule itself, the disposition of such molecules within the solid state can have a profound influence, and different polymorphs can have totally different reactivities. The way in which structure determines crystal packing and thus reactivity in the solid state continues to be an elusive and important goal.

5. Experimental Section

5.1. Photolysis and Product Analysis. A sample of **3-HOBDI** (~80 mg) was spread thin between glass plates and exposed to irradiation from a Hanovia Hg lamp for 1.5 h followed by flipping the plate and continuing irradiation for another 1.5 h. The powder was collected and acetone was used to remove the remaining starting material (4 times). The remaining white solid was allowed to dry on the frit funnel and used for spectroscopy. The yield was ~50% (no attempts were made to maximizing the yield of the product).

5.2. Spectroscopy. Ultraviolet−visible absorption spectra were recorded on a Perkin-Elmer Lambda19 spectrophotometer. Measurements of solid-state photoluminescence were carried out using the front face emission scan mode on a Jobin-Yvon FluoroLog-3 spectrofluorimeter. The entrance/exit slits of the monochromators were adjusted to the proper fluorescence intensity of each sample. Crystalline powder samples were placed between the quartz plates. Fluorescence lifetimes were measured using an Edinburgh Instruments time-correlated single-photon counting (TCSPC) system. In this measurement, two picosecond excitation pulses diode lasers (LDH-P-C-375 and LDH-P-C470) with different wavelengths (372 and 478 nm) were used as excitation light sources. The detection system consisted of a high speed MicroChannel Plate PhotoMultiplier Tube (MCP-PMT, Hamamatsu R3809U-50) and TCSPC electronics.

5.3. Atomic Force Microscopy. In order to more fully characterize the nature of the phototransformation of the **3-HOBDI** crystals, we examined the AFM images of the crystals before and after irradiation. The AFM imaging was completed on a single crystal of **3-HOBDI**-A. For imaging, the crystal was mounted flat on its largest surface using carbon tape on silicon wafer in such a way that part of the crystal was immobilized on the tape while the remaining part was not attached, which allowed for unrestricted movement (a schematic of this assembly is shown in Figure S12 in the SI). The crystal mounting process was done with limited ambient light; however ambient light was not entirely eliminated. From this, preexisting conditions cannot be rigorously excluded. The crystal was irradiated using a Pyrex-filtered Hanovia medium pressure 450 W Hg lamp for 15 min and subjected to AFM analysis. Both segments of the crystal (attached and nonattached) were analyzed. Atomic force microscopy imaging was performed with a model 5500 AFM from Agilent Technologies (Chandler, AZ). The 5500 AFM operates in a "top-down" configuration with the AFM probe mounted on the piezo-scanner for imaging of the sample surface. The AFM was placed in a vibration isolation chamber (Agilent Technologies, Chandler, AZ) and additionally in a Faraday cage in order to reduce environmental vibration and electromagnetic noise. AFM images were postprocessed with the PicoScan 5.3.3 software (Agilent Technologies, Chandler, AZ) for tilt correction or flattening of the image background. For the imaging, Dynamic mode AFM technique was employed. In this technique, the cantilever is oscillated at a certain resonant frequency, and amplitude damping as a result of repulsive tip−sample interaction is monitored. This reduces frictional forces at the sample surface due to the intermittent contact of the tip.

5.4. Polymorph Screening and X-ray Diffraction. Extensive screening of the BDIs from 15 common organic solvents was undertaken to check the existence of polymorphs and solvates (see Table S2 in the SI). The identity of the crystals from different batches was checked by comparison of the cell parameters obtained from limited number of reflections. The samples for X-ray diffraction analysis were prepared by slow evaporation from hexane or ethanol solutions, which always afforded samples of best crystallinity. Except for **3-HOBDI**-A, which always crystallized as very slender long crystals, the BDIs usually appear as large prismatic or blocky crystals. If exposed to room light for a week, some of the crystals (most notably, **3-HOBDI**-A and **2-FBDI**) tend to deform and turn opaque. Therefore, all recrystallized samples were manipulated and stored in the dark (see below) under faint light or red safelight ($\lambda > 660$ nm), including the X-ray measurements.

The X-ray diffraction data were collected in ω-scan mode at room temperature with APEX2 diffractometer (Bruker AXS),[45] using MoKα X-rays obtained from a rotating anode source, a confocal multilayer X-ray mirror as monochromator and CCD area detector. The integrated and scaled[45] data were empirically corrected for absorption effects with SADABS.[46] The structures were solved by using direct methods[47] and refined on F_{obs} with SHELXL.[48] All non-hydrogen atoms were assigned anisotropic displacement parameters. The aromatic protons were set as riding bodies, and the methyl hydrogen atoms were placed at calculated positions, with their rotational angles refined from the electron density. The protons in the hydroxyl groups were kept at calculated distances, but their rotation angles were refined. The crystals of **3-HOBDI**-A are extremely slender (the one used for X-ray diffraction was only 10 μm thick) and tend to curve slightly during the crystallization process (see Figure 1a), even when it is conducted in the dark and at a lowered temperature, which is why the structure could be refined only to $R_1 = 7.14\%$. Although not optimal, this accuracy was considered sufficient for the purpose of analysis of the molecular structure and intermolecular interactions topology. The photoreaction of **3-HOBDI**-A is a homogeneous solid-state process[49] and proceeds simultaneously with the bending throughout any part of the crystals that had been exposed to UV light. Therefore, although the resulting crystal still diffracted as one component, its diffraction pattern was inevitably distorted, which ultimately prevented us from structure determination of the product. The gradual distortion of the diffraction picture was an expected consequence of the continuous progression of the reaction throughout the crystal, although the crystal integrity was preserved. The

(45) *APEX2*, ver. 2.1-4, and *SAINT*, ver. 734A; Bruker AXS Inc.: Madison, Wisconsin, U.S.A., 2007.
(46) Sheldrick, G. M. *SADABS*; University of Göttingen: Göttingen, Germany, 1996.
(47) (a) Sheldrick, G. M. *Acta Crystallogr.* **2008**, *A64*, 112–122. (b) Altomare, A.; Cascarano, G.; Giacovazzo, C.; Guagliardi, A.; Burla, M. C.; Polidori, G.; Camalli, M. *J. Appl. Crystallogr.* **1994**, *27*, 435–436.
(48) Sheldrick, G. M. E. *SHELXL-97*, University of Göttingen, Göttingen, Germany, 1997.
(49) (a) Garcia-Garibay, M. A. *Angew. Chem., Int. Ed.* **2007**, *46*, 8945–8947. (b) Boldyreva, E. In *Reactivity of Solids: Past, Present and Future*; Boldyrev, V. V., Ed.; Blackwell: Cambridge, 1996; pp 141−184.

crystals of **2-FBDI** were refined from a twinned crystal; the twinning was explicitly accounted for in the refinement. Both methyl groups at the imidazole ring of **3-MOBDI** are rotationally disordered, and thus they were included in the model with two positions of equal occupancy. The structure of the partially reacted **3-HOBDI**-C was refined by using several limitations, including constraints (±0.2 Å) on the C8′−N12′ (1.400 Å), N10′−C9′ (1.340 Å) and C9′−O16′ (1.250 Å) bonds. Soft restraint was applied to keep the imidazolone ring atoms of the product flat, and two pairs of atoms were restrained to have similar displacement parameters. The effect on the changes in the crystal color observed by UV irradiation depended on the sample (**2,5-DMBDI** and **4-HOBDI** turn yellow, while **2-FBDI** turns opaque). The attempts to resolve the structure of the photoinduced dimer created in single crystals of the BDIs were not successful, because the crystallinity specimens decreased upon exposure to UV light, as it became evident from the diffraction pattern of **2,5-DMBDI**.

Acknowledgment. L.M.T. and K.M.S. thank the U.S. National Science Foundation (CHE-0809179) for generous financial support. Support for P.N. from the Japanese Science and Technology Agency - JST is also gratefully acknowledged. We thank Dr. Seth Olsen for fruitful discussion and for supplying the Figure S11.

Supporting Information Available: Crystallographic data in CIF and tabular format, details of synthesis, polymorph screening and analytical/spectral characterization (NMR, UV−visible spectra) of the compounds, micrographs of crystals of **3-HOBDI** and **2-FBDI**, schematic of the setup for AFM, and movies showing the photomechanical effects. This material is available free of charge via the Internet at http://pubs.acs.org.

JA100844M